International Journal of Bifurcation and Chaos

PERIODIC ORBITS ASSOCIATED WITH THE LIBRATION POINTS OF THE MASSIVE ROTATING STRAIGHT SEGMENT

VOLODYMYR A. ROMANOV
Photonic Systems Division,
Physical Optics Corporation, 1845 West 205th Street
Torrance, California 90501-1510, USA
vromanov@poc.com

EUSEBIUS J. DOEDEL
Department of Computer Science and Software Engineering,
Concordia University, 1455 boulevard de Maisonneuve O.,
Montréal, Québec H3G 1M8, CANADA
doedel@cse.concordia.ca

Received (to be inserted by publisher)

The massive straight segment, rotating around the axis perpendicular to its center, is a simple alternative for more precise and sophisticated models that take into account the shape and mass density of natural asteroids. In this article we give numerical results for the families of periodic orbits that emanate from the five libration points of massive straight segment, and for some secondary bifurcating families. Possible application and extension of the results to research on the motion of satellites near small irregular-shaped celestial bodies is also discussed. The numerical continuation and bifurcation algorithms we use in our study are based on boundary value techniques, as implemented in AUTO.

Keywords: celestial mechanics; bifurcation analysis; periodic orbits; massive rotating straight segment; missions to asteroids; libration points; numerical continuation.

1. Introduction

The gravitational interaction of the massive rotating straight segment (MRSS) with a central gravitational potential was first considered in [Duboshin, 1959]. In the last decade the MRSS with uniform mass density and its gravitational potential have been studied in many papers [Arribas & Elipe, 2001; Elipe & Lara, 2003, 2004, 2006; Guttiérrez-Romero, *et al.*, 2004; Lara & Scheeres, 2003; Lara, 2003; Riguas, *et al.*, 1999, 2001] as a simple model of small irregular-shaped celestial bodies. Recently the MRSS with parabolic mass density distribution has also been proposed as an enhanced model of the gravitational potential of such bodies [Najid & El Ourabi, 2011, 2012]. Moreover, in [Bartczak & Breiter, 2003] two perpendicular straight segments are described. Their model approximates more accurately the complex gravitational field of irregular, nonspherical celestial bodies, such as small moons or minor asteroids. With the MRSS model and its variations it is relatively easy to calculate periodic orbits of a satellite moving around asteroids approximated by MRSS's. Thus it is a simple alternative for more precise and sophisticated models that

take into account the shape and mass density of natural asteroids. Such more advanced models include that of the homogeneous rotating gravitating triaxial ellipsoid [Doedel & Romanov, 2012; Hu & Scheeres, 2002; Scheeres, 1994; Scheeres, *et al.*, 1996, 2000]. Basic families of periodic orbits that emanate from the libration points of the rotating gravitating triaxial ellipsoid, as well as some secondary bifurcating families, are computed in [Doedel, Romanov, 2012] using boundary value techniques as implemented in the AUTO software [Doedel & Oldeman, 2011]. The same approach was used in [Doedel *et al.*, 2007; Dichmann, *et al.*, 2003; Doedel, *et al.*, 2003] to compute periodic orbits in the Circular Restricted 3-Body Problem. In the current paper we use this approach to determine families of periodic orbits for the MRSS. The techniques used in [Doedel & Romanov, 2012] can also be generalized to the computation of periodic orbits for gravitational potentials of natural asteroids and elliptical galaxies [Davoust, 1983, 1986] of irregular shape and nonhomogeneous mass density. Such work could be of much interest in current research on asteroid space missions and in astrophysics.

2. Libration Points of the MRSS and their Properties

Suppose we have a finite straight segment along the axis OX of length $2a$, mass M, and linear mass density $\rho \equiv M/(2a)$ (Fig. 1a). Also suppose that this straight segment rotates uniformly around the OZ axis with angular rotation velocity ω, together with the frame of reference $OXYZ$. The gravitational potential of the segment at any point (X, Y, Z), as given in [Duboshin, 1959; Elipe & Lara, 2003, 2004, 2006; Riguas, *et al.*, 1999, 2001], is equal to

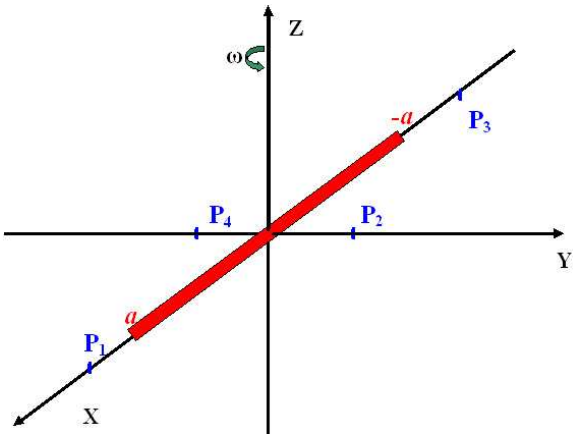

(a) The MRSS of length $2a$ and its four libration points P_i, $(i = 1, \cdots, 4)$, in the rotating frame of reference $OXYZ$, with angular rotation velocity ω.

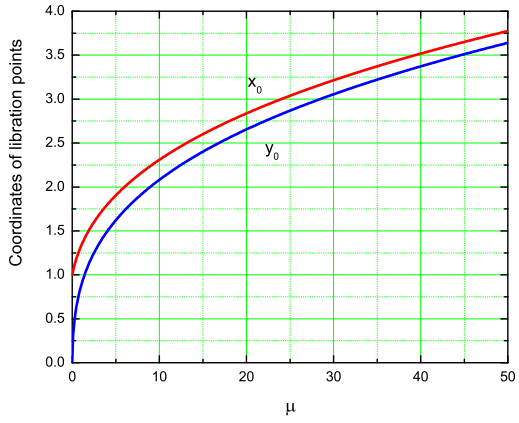

(b) Coordinates of the libration points x_0 (***red***) and y_0 (***blue***) of the MRSS, as functions of its "rotating-gravitating" parameter μ.

Fig. 1

$$V \equiv V(X,Y,Z) = G\rho \int_{-a}^{a} \frac{dt}{\sqrt{(X-t)^2+Y^2+Z^2}} = \frac{GM}{2a} \ln\left(\frac{\sqrt{(X+a)^2+Y^2+Z^2}+(X+a)}{\sqrt{(X-a)^2+Y^2+Z^2}+(X-a)}\right) \tag{1}$$

where $G = 6.67 \cdot 10^{-11}\ m^3 s^{-2} kg^{-1}$ is the constant of gravity. Let

$$R_1 = \sqrt{(X-a)^2+Y^2+Z^2} \tag{2}$$

be the distance from the point (X, Y, Z) to the end of the straight segment, with coordinates $X_{01} = -a$, $Y_{02} = 0$, $Z_{02} = 0$, and let

$$R_2 = \sqrt{(X+a)^2 + Y^2 + Z^2} \tag{3}$$

be the corresponding distance to the other end of the MRSS, with coordinates $X_{02} = a$, $Y_{02} = 0$, $Z_{02} = 0$. Then the potential (1) can be rewritten as

$$V(X,Y,Z) = -\frac{GM}{2a} \ln\left(\frac{R_1 + R_2 + 2a}{R_1 + R_2 - 2a}\right) . \tag{4}$$

In the rotating frame of reference $OXYZ$ the equations of motion of an infinitesimal body in the gravitational field of the MRSS are

$$\begin{aligned} X'' - 2\omega Y' - \omega^2 X &= \frac{\partial V}{\partial X} , \\ Y'' + 2\omega X' - \omega^2 Y &= \frac{\partial V}{\partial Y} , \\ Z'' &= \frac{\partial V}{\partial Z} , \end{aligned} \tag{5}$$

where prime $'$ denotes the time derivative. The partial derivatives of the gravitational potential (4) are

$$\begin{aligned} \frac{\partial V}{\partial X} &= \frac{GM}{2a} \frac{X}{(R_1+R_2)R_1R_2} , \\ \frac{\partial V}{\partial Y} &= \frac{GM}{2a} \frac{Y}{(R_1+R_2)R_1R_2} \left(1 - \frac{4a^2}{(R_1+R_2)^2}\right)^{-1} , \\ \frac{\partial V}{\partial Z} &= \frac{GM}{2a} \frac{Z}{(R_1+R_2)R_1R_2} \left(1 - \frac{4a^2}{(R_1+R_2)^2}\right)^{-1} . \end{aligned} \tag{6}$$

We introduce normalized coordinates $x \equiv X/a$, $y \equiv Y/a$, and $z \equiv Z/a$, so that the normalized length of the segment is equal to 2. We can then rewrite the equations of motion (4) as

$$\begin{aligned} x'' - 2y' &= x\left(1 - \frac{2\mu}{p}\right) , \\ y'' + 2x' &= y\left(1 - \frac{2\mu}{p\,(1-s)}\right) , \\ z'' &= -\,z\frac{2\mu}{p\,(1-s)} , \end{aligned} \tag{7}$$

where

$$\mu \equiv \frac{GM}{\omega^2 a^3} , \tag{8}$$

$$p \equiv ((r_1 + r_2) r_1 r_2) \ , \quad s \equiv \frac{4}{(r_1+r_2)^2} , \tag{9}$$

$$r_1 \equiv \sqrt{(x-1)^2 + y^2 + z^2} \ , \quad r_2 \equiv \sqrt{(x+1)^2 + y^2 + z^2} . \tag{10}$$

Equation (7) yields four libration points [Markeyev, 1978], namely, $L_1 = (x_0, 0, 0)$, $L_2 = (0, y_0, 0)$, $L_3 = (-x_0, 0, 0)$, and $L_4 = (0, -y_0, 0)$, where the coordinates x_0 and y_0 are solutions of the equations

$$\begin{aligned} x_0^3 - x_0 - \mu = 0 \ , \\ y_0^2\sqrt{(1+y_0^2)} - \mu = 0 \ . \end{aligned} \tag{11}$$

For $0 \le \mu < +\infty$ we have from (11) that $1 \le x_0 < +\infty$, and $0 \le y_0 < +\infty$. Solutions of Eqs. (11) are shown graphically in Fig. 1b.

The Jacobian of the first-order system corresponding to (7) at the libration points $L_1 = (x_0, 0, 0)$, and $L_3 = (-x_0, 0, 0)$ is given by

$$J \ = \ \begin{pmatrix} 0 & 2 & 0 & 1+f_{xx} & 0 & 0 \\ -2 & 0 & 0 & 0 & 1+f_{yy} & 0 \\ 0 & 0 & 0 & 0 & 0 & f_{zz} \\ 1 & 0 & 0 & 0 & 0 & 0 \\ 0 & 1 & 0 & 0 & 0 & 0 \\ 0 & 0 & 1 & 0 & 0 & 0 \end{pmatrix} \ , \tag{12}$$

where

$$\begin{aligned} f_{xx} &\equiv \frac{\partial^2 V(x,y,z)}{\partial x^2}|_{(x=\pm x_0,\ y=0,\ z=0)} = \frac{2x_0^2}{x_0^2-1} \ , \\ f_{yy} &\equiv \frac{\partial^2 V(x,y,z)}{\partial y^2}|_{(x=\pm x_0,\ y=0,\ z=0)} = -\frac{x_0^2}{x_0^2-1} \ , \\ f_{zz} &\equiv \frac{\partial^2 V(x,y,z)}{\partial z^2}|_{(x=\pm x_0,\ y=0,\ z=0)} = -\frac{x_0^2}{x_0^2-1} \ . \end{aligned} \tag{13}$$

It follows that we have two separate equations for the six eigenvalues $\sigma_{1,2,3,4,5,6}$ of the Jacobian (12), namely,

$$\sigma^2 = f_{zz} \ , \tag{14}$$

and

$$\sigma^4 - (f_{xx} + f_{yy} - 2)\,\sigma^2 + (1 + f_{xx} + f_{yy} + f_{xx}f_{yy}) = 0 \ . \tag{15}$$

Equation (14) has two purely imaginary conjugate roots $\sigma_{1,2} = \pm\sqrt{f_{zz}}$, because $f_{zz} < 0$. Correspondingly one family of periodic orbits emanates from each of the libration points P_1 and P_3. The eigenvectors of the Jacobian corresponding to these two eigenvalues are

$$\mathbf{e}_1 = (0, 0, \sqrt{f_{zz}}, 0, 0, 1)^T, \quad \mathbf{e}_2 = (0, 0, -\sqrt{f_{zz}}, 0, 0, 1)^T. \tag{16}$$

The corresponding orbit families are vertical, which is consistent with the fact that $\mathbf{e}_1$ and $\mathbf{e}_2$ have non-zero z-coordinate and non-zero z-velocity component ($z = \pm\sqrt{f_{zz}},\ z' = 1$), whereas the other components are zero.

The solutions of Eqn. (15) are

$$\sigma_{3,4}^2 = \frac{x_0^2+1}{x_0^2-1} \ , \quad \sigma_{5,6}^2 = -\frac{2x_0^2-1}{x_0^2-1} \ , \tag{17}$$

so that we have two real and two purely imaginary conjugate values of σ, because the right hand side of the first equation in (17) is positive and for the second equation it is negative. The corresponding eigenvectors lie in the Oxy-plane and are given by

$$\begin{aligned} \mathbf{e}_3 = (\tilde{e}_{1x}, \tilde{e}_{1y}, 0, e_{1x}, 1, 0)^T, \quad \mathbf{e}_4 = (\tilde{e}_{1x}, -\tilde{e}_{1y}, 0, -e_{1x}, 1, 0)^T, \\ \mathbf{e}_5 = (\tilde{e}_{2x}, \tilde{e}_{2y}, 0, e_{2x}, 1, 0)^T, \quad \mathbf{e}_6 = (\tilde{e}_{2x}, -\tilde{e}_{2y}, 0, -e_{2x}, 1, 0)^T. \end{aligned} \tag{18}$$

The non-zero coordinates of the eigenvectors $\tilde{e}_{ix}$, $\tilde{e}_{iy}$, e_{ix}, and e_{iy} $(i = 1, 2)$ are real and can be expressed in terms of x_0 or μ (Eqs. (17) and (11)). Correspondingly we have a bifurcating family of planar periodic orbits. It also follows that the libration points P_1 and P_3 are saddle points.

For the libration points $P_2 = (0, y_0, 0)$ and $P_4 = (0, y_0, 0)$ the corresponding equations for the eigenvalues $\rho_{1,2,3,4,5,6}$ of the Jacobian are

$$\rho^2 = g_{zz} \ , \tag{19}$$

and

$$\rho^4 - (g_{xx} + g_{yy} - 2)\,\rho^2 + (1 + g_{xx} + g_{yy} + g_{xx}g_{yy}) = 0 \ . \tag{20}$$

where

$$\begin{aligned} g_{xx} &\equiv \frac{\partial^2 V(x,y,z)}{\partial x^2}|_{(x=0,\ y=\pm y_0,\ z=0)} = -\ \frac{y_0^2}{y_0^2+1} \ , \\ g_{yy} &\equiv \frac{\partial^2 V(x,y,z)}{\partial y^2}|_{(x=0,\ y=\pm y_0,\ z=0)} = -1 + \frac{(3y_0^2+2)}{y_0^2+1} \ , \\ g_{zz} &\equiv \frac{\partial^2 V(x,y,z)}{\partial z^2}|_{(x=0,\ y=\pm y_0,\ z=0)} = -1 \ . \end{aligned} \tag{21}$$

Equation (19) has two purely imaginary conjugate roots $\sigma_{1,2} = \pm i$, giving rise to one vertical family of periodic orbits emanating from each of P_2 and P_4. Equation (20) has two pairs of complex conjugate roots, both of which have positive real parts for $0 \leq y_0 \leq \sqrt{5 + 4\sqrt{2}} \approx 3.264483765$, or equivalently for $0 \leq \mu \leq 18 + 13\sqrt{2} \approx 36.38477631$. This means that for such μ values no periodic orbit families emanate from the libration points P_2 and P_4, and that these points are linearly unstable. If $\mu \gtrsim 36.38477631$ then Eq. (20) has two pairs of purely imaginary roots. In this case there are two planar periodic orbit families that emanate from each of P_2 and P_4, and these points are centers.

In summary we have found that

1) for any value of μ the libration points P_1 and P_3 are saddles, and from each of these emanate two periodic orbit families (one planar and one vertical),

while for the libration points P_2 and P_4 we have two cases:

2a) for $0 \leq \mu \lesssim 36.38477631$ one (vertical) periodic orbit family emanates from each of P_2 and P_4; these points are unstable foci;

2b) for $\mu \gtrsim 36.38477631$ three periodic orbit families (two planar and one vertical) emanate from each of P_2 and P_4; these points are centers.

The linear and nonlinear stability of the libration points of the MRSS is studied in detail in [Riaguas, *et al.*, 2001].

3. Elemental Periodic Orbits of the MRSS with $\mu \lesssim 36.38$

In this section we present primary periodic orbit families that emanate directly from the libration points, and also some secondary orbit families bifurcating from the primary families. All orbit families are calculated for two representative values of the parameter μ, namely, $\mu = 1.0$ and $\mu = 30.0$. From the conclusion of Section 2 we know that for each of these two values of μ, two orbit families emanate from each of P_1 and P_3, and one orbit family emanates from each of P_2 and P_4, as shown in the schematic bifurcation diagrams in Fig. 2. Secondary orbit families that bifurcate from the primary families are also indicated in this bifurcation diagram.

Each point on a line in the bifurcation diagram in Fig. 2 (and later also in Fig. 8) represents a periodic orbit with its associated period. Along the families of periodic solutions there are various branch points.

Table 1: Abbreviations used for orbit families and branch points. Note that not all of these items need to be present for specific values of the parameter μ.

Symbol	Definition	Example
P_i	The libration points ($i = 1, \cdots, 4$)	Fig. 2a
A*ij*	The *i*th Axial family connecting **L***i* and **V***i* ($\boldsymbol{i} = 1, \cdots, 4$; $\boldsymbol{j}$ = 1,2)	Fig. 3e
D*ij*	The *j*th non-planar orbit family bifurcating from **V***i*	Fig. 3f
E0	The non-planar orbit family connecting **L1** and **L3**	Fig. 3d
L*i*	The planar Lyapunov family that emanates from P_i ($\boldsymbol{i} = 1, \cdots, 4$)	Fig. 3a
R0	The planar family connecting the families **L***i* ($\boldsymbol{i}$= $1, \cdots, 4$)	Fig. 9f
S2/S4	The planar families that emanate from P_2/P_4	Fig. 9e
T2/T4	The planar families that bifurcate from **L0** and terminate in a homoclinic connection with P_2/P_4.	Fig. 7a
V*i*	The Vertical family that emanates from P_i ($\boldsymbol{i} = 1, \cdots, 4$)	Fig. 3b
$\mathbf{L}_{ij}$	Branch point j along the family **L***i*	Fig. 2a
$\mathbf{V}_{ij}$	Branch point j along the family **V***i*	Fig. 2a

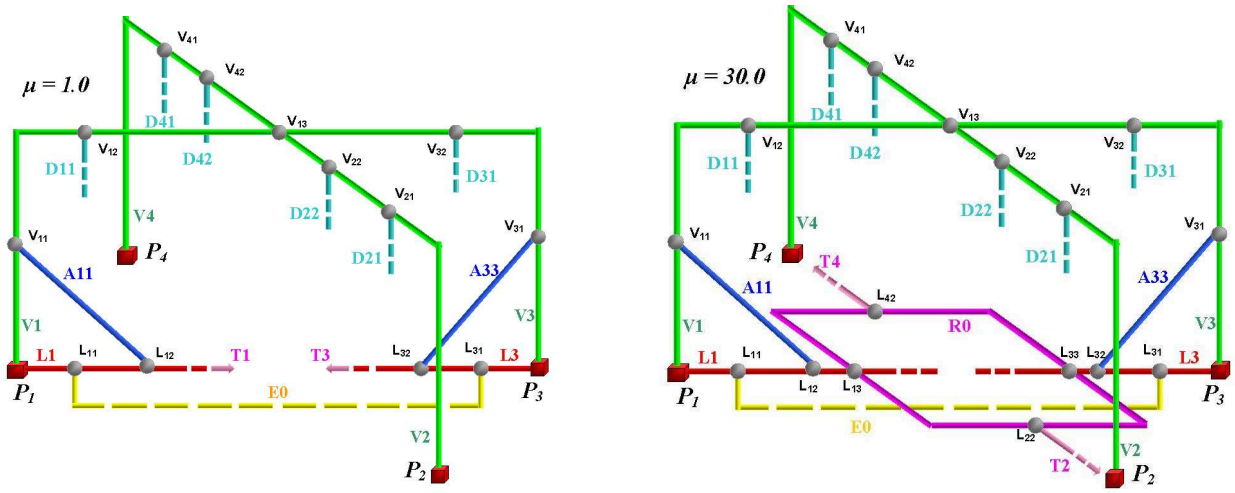

(a) 3D bifurcation diagram for the MRSS with $\mu = 1$.

(b) 3D bifurcation diagram for the MRSS with $\mu = 30$.

Fig. 2: 3D bifurcation diagrams. The red cubes with black labels denote libration points. The color lines with correspondingly colored labels represent orbit families. The gray spheres with black labels indicate branch points. A detailed description of orbit families drawn as dashed lines is not included in this paper. Arrows indicate homoclinic orbits.

In this paper we use the term *branch point* to denote transcritical and pitchfork bifurcations, thereby excluding period-doubling, torus, and subharmonic bifurcations. At a branch point, distinct periodic solution families intersect, with identical orbit and identical minimal period at the point of intersection. Apart from some special cases, we do not present results for solution families that bifurcate from period-doubling and subharmonic bifurcations. However, the solution structure that we present here can be viewed as a "skeleton" from which many other solutions may be reached [Doedel *et al.*, 2007]. Families that exist, but for which we do not present details, are drawn as dashed lines. The notation used to denote orbit families and branch points is summarized in Table 1.

Due to symmetry, the libration points P_1 and P_3 give rise to symmetry-related families of periodic orbits, and similarly for P_2 and P_4. For this reason we only describe the families that emanate from P_1 and P_2. In all diagrams that show actual orbits, *e.g.*, Figs. 3a-3f, stable orbits are blue, unstable orbits red, and orbits that correspond to branch points are green. Branch points are represented by gray spheres in the bifurcation diagrams. The small magenta cubes represent the libration points: P_1, and P_3 on the Ox axis, and P_2, and P_4 on the Oy axis. The straight segment is displayed as a cylinder of color cyan. Figures such as 3a-3f, *etc.*, show several orbits drawn together. Individual orbits are closed curves (planar or 3D), possibly containing loops.

The local stability of a periodic orbit can be analyzed using Floquet theory; in the current context see, for example, [Celetti, 2010]. Suppose $\boldsymbol{X}(t)$ is a periodic solution of period T of the general n-dimensional problem $\boldsymbol{X}'(t) = \boldsymbol{F}(\boldsymbol{X}(t), \lambda)$, where λ is a scalar parameter. Introduce the matrix $\Phi(T, \lambda)$, as the solution of the initial-value problem

$$\Phi' = \frac{\partial \boldsymbol{F}(\boldsymbol{X}, \lambda)}{\partial \boldsymbol{X}} \, \Phi \ , \qquad \Phi(0, \lambda) = I \ , \tag{22}$$

where I is the identity matrix. The matrix $\Phi(T, \lambda)$ has n eigenvalues: $\nu_1, \cdots, \nu_n$, called Floquet multipliers. Due to translation invariance and the fact that the equations are conservative, two multipliers equal unity, say, $\nu_1 = 1$, $\nu_2 = 1$. The remaining $n - 2$ eigenvalues determine the stability: we will call the periodic solution $\boldsymbol{X}$(t) "stable" if $\mid \nu_j \mid \leq 1$ for $j = 1, \cdots, n$, and unstable if $\mid \nu_j \mid > 1$ for some j. Thus in our numerical results, we call an periodic orbit (linearly) stable if all Floquet multipliers are on or inside the unit circle. In AUTO the Floquet multipliers are determined at neglible computational cost as part of the boundary value solution procedure for computing a periodic orbit.

3.1. *The case $\mu = 1.0$*

The bifurcation diagram for $\mu = 1.0$ is shown in Fig. 2a. Two orbit families emanate from each libration point P_1 and P_3, namely, the planar Lyapunov orbit family **L1**/**L3** for which Fig. 3a shows representative orbits, and the non-planar Vertical orbit family **V1**/**V3** (Fig. 3b). Only one non-planar family of periodic orbits emanates from each of the libration points P_2 and P_4, namely, the Vertical orbits **V2**/**V4**, for which representative orbits are shown in Fig. 3c. Below we discuss these primary families and some secondary families in more detail.

3.1.1. *The Lyapunov orbit family **L1***

As seen in Fig. 2a, the first branch point $\mathbf{L}_{11}$ encountered along the Lyapunov orbit family **L1** leads to the non-planar orbit family **E0** (Fig. 3d), which connects **L1** to its symmetry partner, the Lyapunov family **L3**. The second branch point $\mathbf{L}_{12}$ along **L1** leads to the Axial orbit family **A11** (Fig. 3e), which connects **L1** to **V1**. The Lyapunov family **L1** itself terminates in a symmetric heteroclinic cycle that approaches each of the libration points P_2 and P_4 as its period tends to infinity. There are further branch points along **L1** as it approaches the terminating heteroclinic cycle that are not indicated in Fig. 2a, but that do appear as unlabeled green orbits in Fig. 3a. The families that emanate from these additional branch points appear to lead to asymmetric cycles heteroclinic to P_2 and P_4. A discussion of similar connections is given in [Doedel *et al.*, 2007]. The orbit families **L1** and **A11** are unstable, while **E0** contains stable portions (Fig. 3d). The orbit family **E0** contains branch points, whose emanating families we have not investigated in detail.

3.1.2. *The Vertical orbit family **V1***

The Vertical orbit family **V1** (Fig. 3b) is completely unstable and has three branch points $\mathbf{V}_{11}$ - $\mathbf{V}_{13}$ where **V1** connects to: (*i*) the non-planar Axial orbit family **A11**, which in turn connects to the Lyapunov orbit family **L1**; (*ii*) the non-planar orbit family **D11** (Fig. 3f); (*iii*) the other Vertical orbit families, namely, **V2** (Fig. 3c), **V3**, and **V4**. The orbit family **D11** terminates in *collision orbits*, *i.e.*, orbits for which the velocity components tend to infinity at some point along the orbit. The detailed structure of such orbit family needs further investigation.

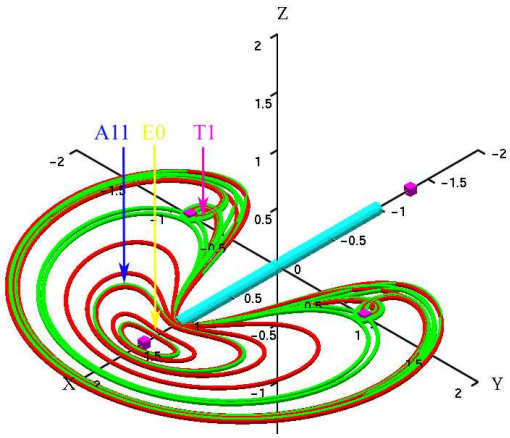

(a) The planar Lyapunov orbit family **L1** that emanates from the libration point P_1; $\mu = 1.0$.

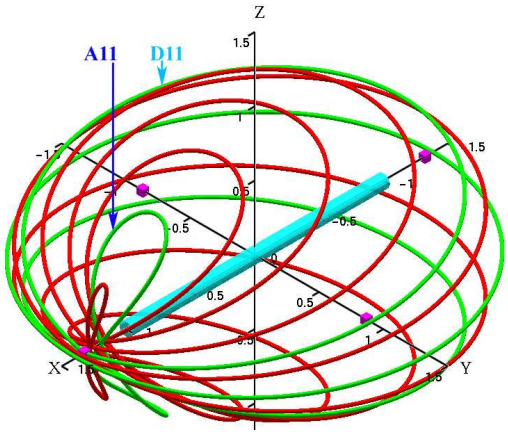

(b) The Vertical orbit family **V1** that emanates from the libration point P_1; $\mu = 1.0$.

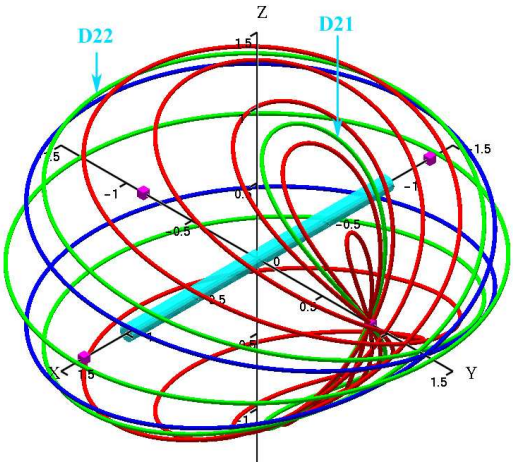

(c) The Vertical orbit family **V2** that emanates from the libration point P_2; $\mu = 1.0$.

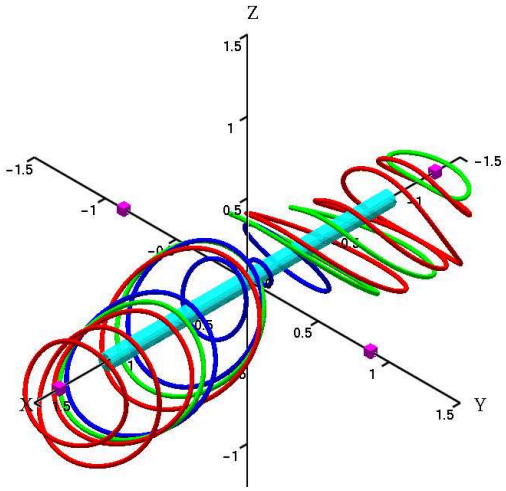

(d) The non-planar orbit family **E0** that bifurcates from the Lyapunov orbit family **L1** and connects to the family **L3**; $\mu = 1.0$.

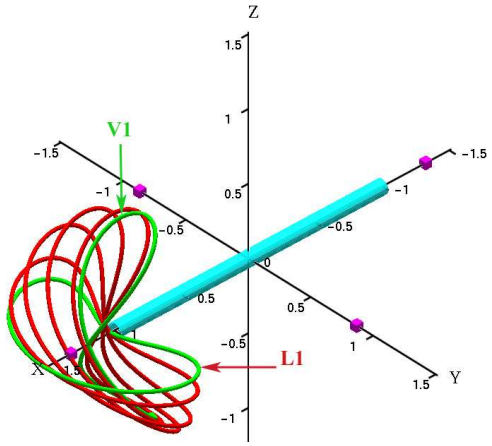

(e) The Axial orbit family **A11** that forms a connection between the Lyapunov orbit family **L1** and the Vertical orbit family **V1**; $\mu = 1.0$.

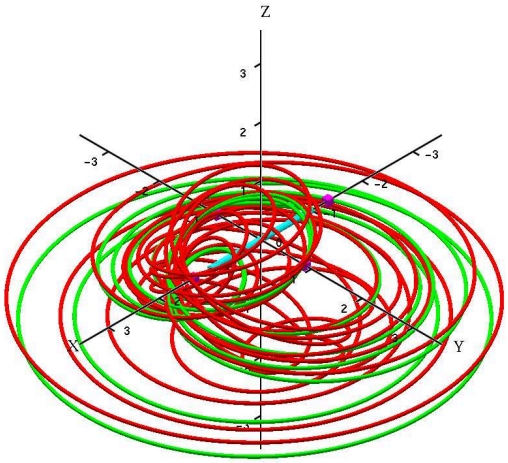

(f) The orbit family **D11** that bifurcates from the Vertical orbit family **V1**; $\mu = 1.0$.

Fig. 3

3.1.3. *The Vertical orbit family* ***V2***

This orbit family has three branch points $\mathbf{V}_{21}$, $\mathbf{V}_{22}$, and $\mathbf{V}_{13}$ where **V2** connects to: (*i*) the non-planar orbit family **D21** (Fig. 4a); (*ii*) the non-planar orbit family **D22** (Fig. 4b); (*iii*) the other Vertical orbit families, namely, **V1** (Fig. 3b), **V3**, and **V4**. The orbit family **V2** is stable between the second and the third branch point. The orbit families **D21** and **D22** terminate in *collision orbits*; the detailed structure of these orbit families requires further investigation.

3.2. *The case* $\mu = 30.0$

The bifurcation diagram for $\mu = 30$ is shown in Fig. 2b. As for the case $\mu = 1$ there are two primary orbit families that emanate from each of the libration points P_1 and P_3 (a Lyapunov family **L1**/**L3** and a Vertical family **V1**/**V3**). Also similar to the case $\mu = 1$, only one primary orbit family, namely **V2**/**V4**, emanates from each of the libration points P_2 and P_4. However, new secondary orbit families can be reached via bifurcations from **L1**/**L3**, namely **R0** and **T2**/**T4**, making the bifurcation diagram differ from the diagram for $\mu = 1$.

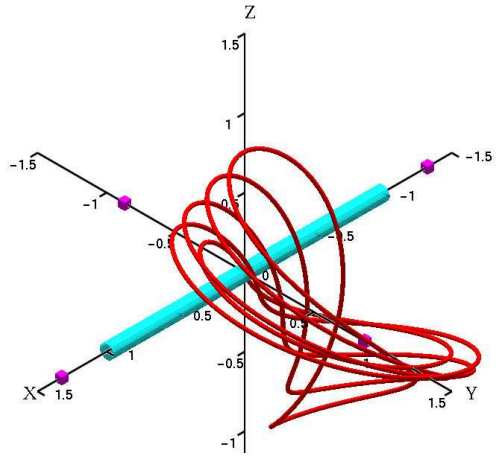

(a) The orbit family **D21** that bifurcates from the Vertical orbit family **V2** and terminates in a collision orbit; $\mu = 1.0$.

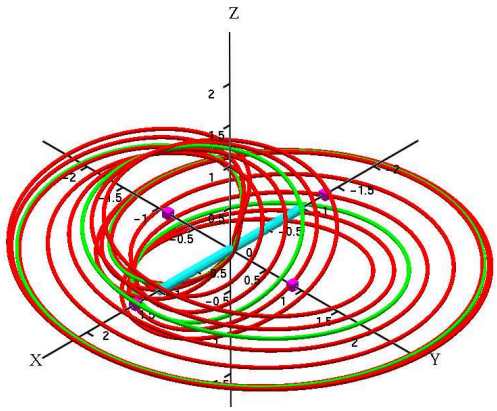

(b) The orbit family **D22** that bifurcates from the Vertical orbit family**V2** and terminates in a collision orbit; $\mu = 1.0$.

Fig. 4

3.2.1. *The Lyapunov orbit family* ***L1***

The topological structure of the planar orbit families (*i.e.*, families whose orbits lie in the xy-plane) in the bifurcation diagram in Fig. 2b differs from the case $\mu = 1.0$ in that the Lyapunov orbit family **L1** (Fig. 6a) has an additional branch point $\mathbf{L}_{13}$, connecting it to a planar orbit family **R0** (Fig. 6b), which in turn connects to a planar orbit family **T4** (Figs. 7a, 7b). Furthermore, the family **R0** connects **L1** to its symmetry partner **L3**. In this case the Lyapunov orbit family **L1** does not terminate in an infinite period orbit. However, infinite period connections to P_2 and P_4 can be reached via **R0** and **T2**/**T4**. We note that **L1** has a small region of stable orbits that pass through a vicinity of the libration points P_2 and P_4 (Fig. 6a), and that most of the orbits along **R0** are stable. The families **T2** and **T4** also contain regions of stable orbits (Figs. 7a, 7b).

3.2.2. *The Vertical orbit families* ***V1*** *and* ***V2***

The non-planar Vertical orbit families **V1**, **V2**, **V3**, **V4** in Fig. 2b, and their bifurcating families **E0**, **A11**, **A33**, **D11**, **D21**, **D22**, *etc.*, are similar to the previous case of $\mu = 1.0$ (Fig. 2a, and Fig. 3b - Fig. 4b). Most

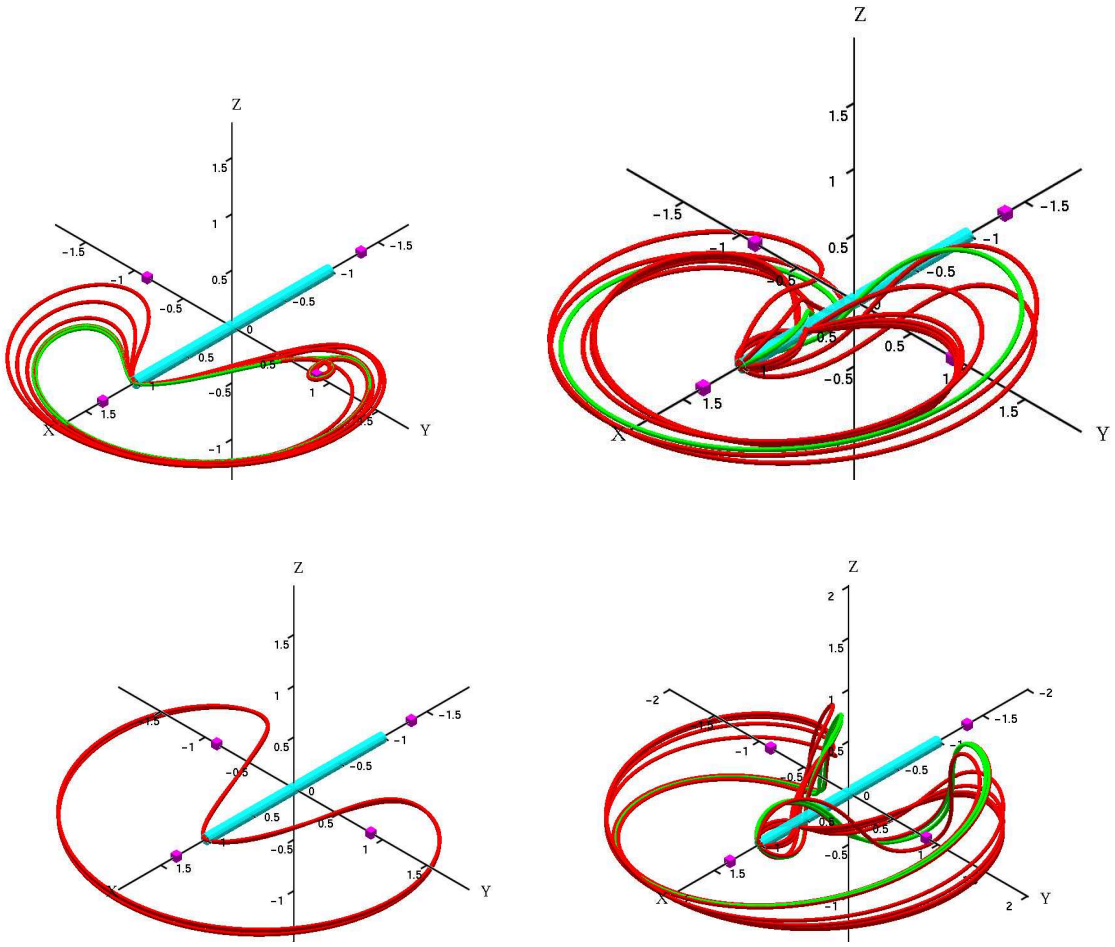

Fig. 5: Some planar and non-planar orbit families bifurcating from the Lyapunov orbit family **L1** ($\mu = 1.0$).

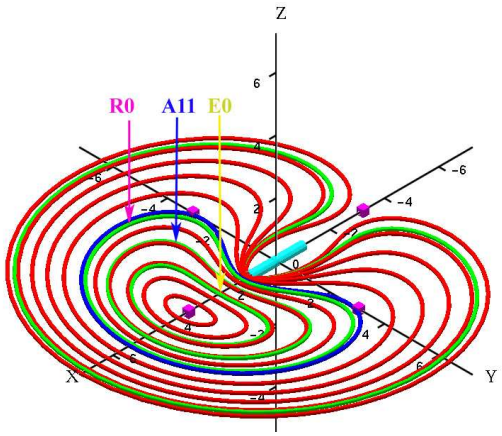

(a) The planar Lyapunov orbit family **L1** that emanates from the libration point P_1; $\mu = 30.0$.

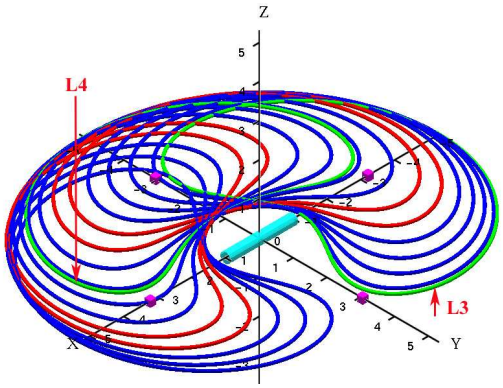

(b) The planar orbit family **R0** that connects the Lyapunov orbit families **L1** and **L3**; $\mu = 30.0$.

Fig. 6

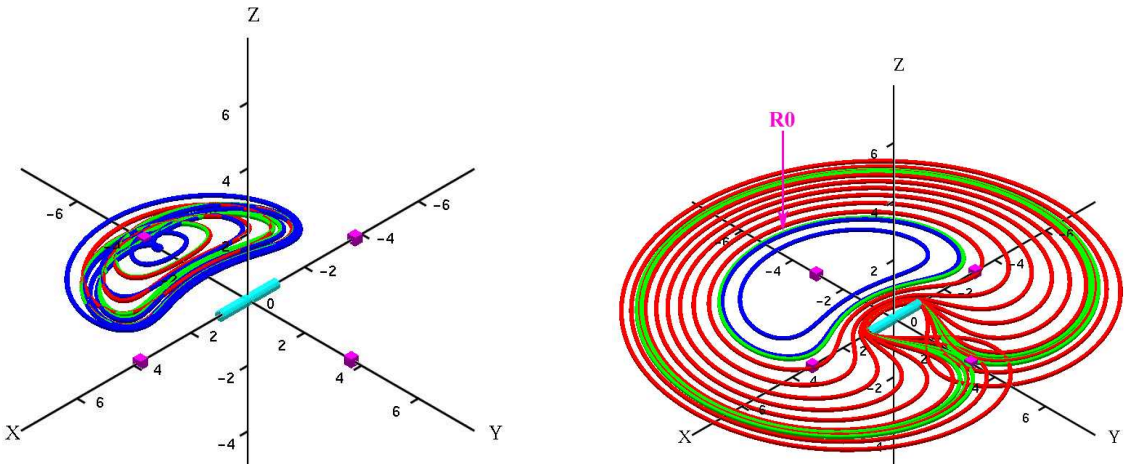

(a) The inner part of the planar orbit family **T4** that bifurcates from **R0**; $\mu = 30.0$.

(b) The outer part of the planar orbit family **T4**; $\mu = 30.0$.

Fig. 7

orbits along **V1** and along the families bifurcating from it are unstable, although some of these families contain stable parts. The orbit family **V2** contains a region of stable orbits between the second and the third bifurcation point.

4. Elemental Periodic Orbits of the MRSS with $\mu > 36.38$

The bifurcation diagram for this case, given in Fig. 8, is topologically the same for all $\mu \gtrsim 36.38$. As for the cases $\mu = 1.0$ and $\mu = 30.0$, there are two orbit families that emanate from each of the libration points P_1 and P_3: one Lyapunov family **L1/L3** (Fig. 9a), and one Vertical family **V1/V3** (Fig. 9b). However, for each libration point P_2 and P_4 there are now three bifurcating families: a Vertical family **V2/V4** (Fig. 9d), and two planar families, namely the Lyapunov orbit family **L2/L4** (Fig. 9c) and the short-period orbit family **S2/S4** (Fig. 9e).

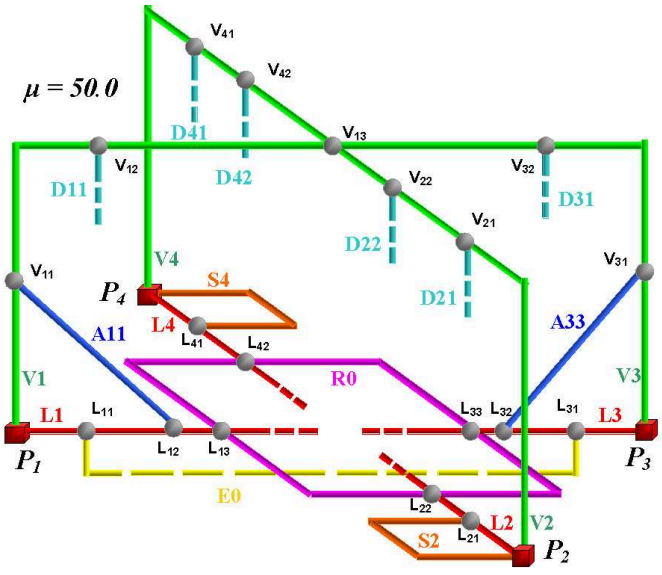

Fig. 8: 3D bifurcation diagram for the MRSS with $\mu = 50.0$.

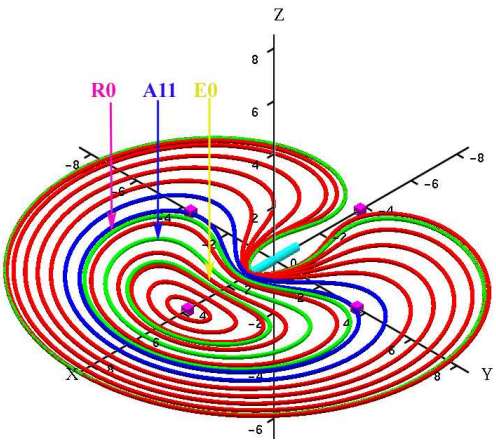

(a) The planar Lyapunov orbit family **L1** that emanates from the libration point P_1; $\mu = 50.0$.

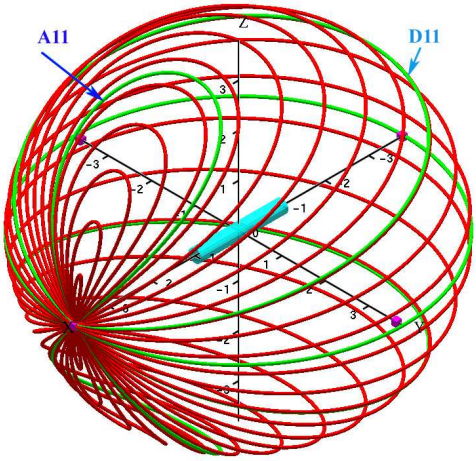

(b) The Vertical orbit family **V1** that emanates from the libration point P_1; $\mu = 50.0$.

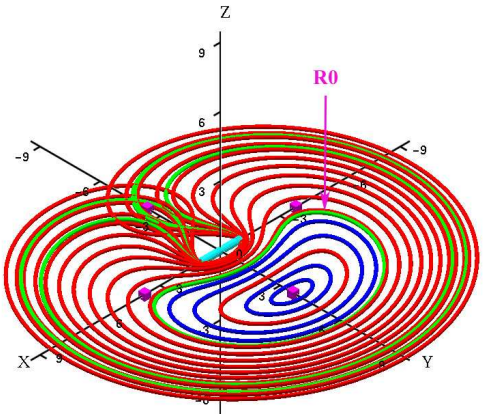

(c) The planar Lyapunov orbit family **L2** that emanates from the libration point P_2; $\mu = 50.0$.

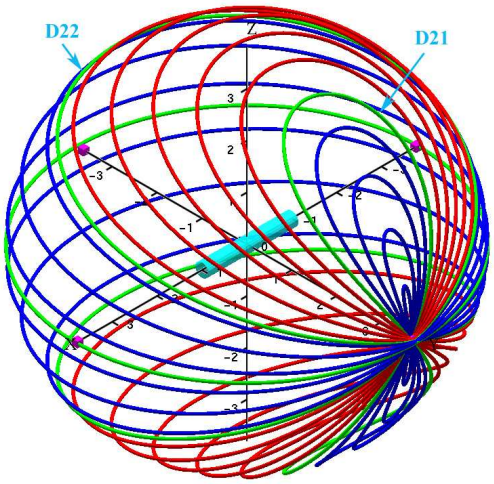

(d) The Vertical orbit family **V2** that emanates from the libration point P_2; $\mu = 50.0$.

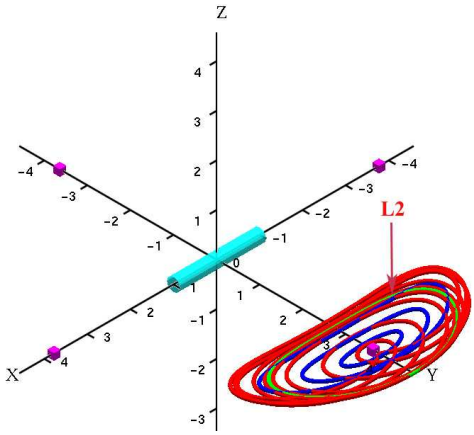

(e) The planar orbit family **S2** that emanates from the libration point P_2; $\mu = 50.0$.

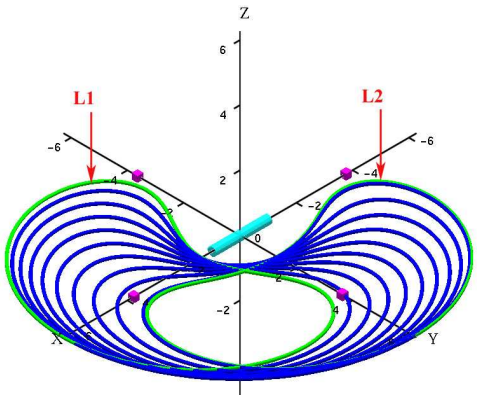

(f) The planar orbit family **R0** that connects the Lyapunov orbit families **L1**, **L2**, **L3**, and **L4**; $\mu = 50.0$.

Fig. 9

4.1.1. *The Lyapunov orbit family* ***L2***

The bifurcation diagram in Fig. 8 has significant changes compared to the case $\mu < 36.38$. The planar Lyapunov orbit family **L2** (Fig. 9c) that emanates from P_2 contains branch points, as does its symmetry partner **L4**. The first two of these, $\mathbf{L}_{21}$ and $\mathbf{L}_{22}$, connect **L2**: (*i*) through a period-doubling bifurcation to the short-period planar orbit family **S2** that also emanates from P_2; (*ii*) to the planar orbit family **R0** (Fig. 9f) which interconnects all four Lyapunov orbit families **L1** - **L4**, as in the case $\mu = 30.0$. There are no connections between **L2** and **V2** via an Axial orbit family, such as the family **A22** in the case $\mu = 30.0$. The orbit family **L2** has additional branch points not shown in Fig. 8, which connect **L2** to other planar and non-planar orbit families (Fig. 10). A more detailed structure of the orbit family **L2** merits further investigation.

4.1.2. *The short-period planar orbit family* ***S2***

The short-period planar family **S2** (Fig. 9e) and its symmetry partner **S4** have one branch point $\mathbf{L}_{21}$, connecting **S2** to the Lyapunov family **L2** through a period-doubling bifurcation. Generally, the periods of the **S2**/**S4** orbits are about one-half the periods of the Lyapunov orbits **L2**/**L4**.

4.1.3. *The Vertical orbit families* ***V1*** *and* ***V2***

The bifurcation diagram in Fig. 8 shows that its non-planar part, *i.e.*, orbit families **V1**, **V2**, **V3**, **V4** (Fig. 9b, Fig. 9d), and orbit families bifurcating from them, namely, **E0**, **A11**, **A33**, **D11**, **D21**, **D22**, *etc.*), are similar to the previous case (Fig. 2). For example, the orbit family **V2** here also has two regions of stable orbits (Fig. 9d).

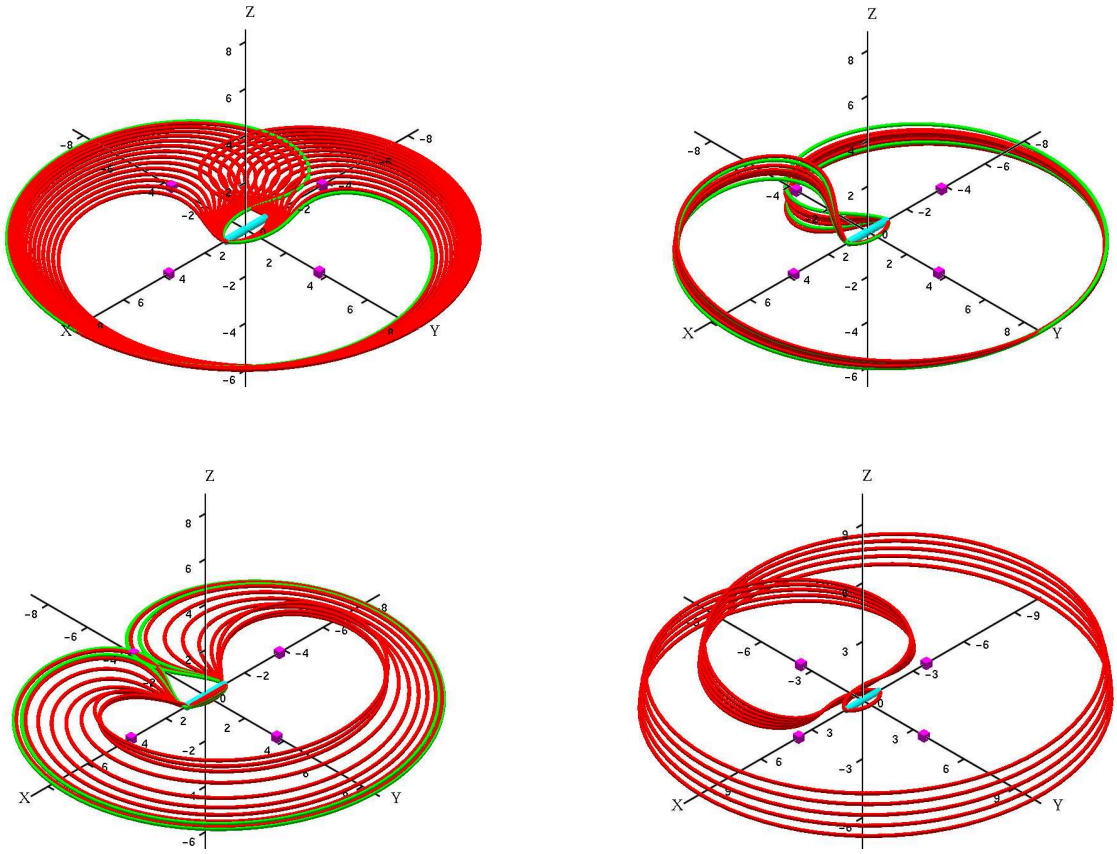

Fig. 10: Some planar and non-planar families bifurcating from the Lyapunov orbit family **L2**; $\mu = 50.0$.

5. Discussion

The topological structure of the bifurcation diagram of the MRSS is complex, as is the structure of the bifurcation diagram of the Rotating Gravitating Triaxial Ellipsoid [Doedel & Romanov, 2012]. A diverse set of primary orbit families emanate from the libration points of the MRSS, and a wealth of secondary and tertiary orbit families can be reached via the primary families. Although the detailed structure of some of these families merits further investigation, our present results clarify the structure of the basic orbit families. Apart from its theoretical interest, a good reason for studying a simple model like the MRSS is that provides a first approximation to irregularly shaped celestial bodies, including many small asteroids and planetary satellites ([Doedel & Romanov, 2012]). While the Rotating Gravitating Triaxial Ellipsoid approximation [Doedel & Romanov, 2012] may be more suitable for many such cases, it does require much more computer time. Thus the MRSS serves as a coarse model for the determination of periodic orbit families associated with small celestial bodies.

The results presented here and in [Doedel & Romanov, 2012; Doedel *et al.*, 2007] may also be a starting point for similar studies of more realistic models of asteroids and other small celestial bodies [Britt *et al.*, 2002; Cellino *et al.*, 1989; Mitchell *et al.*, 1998; Miller *et al.*, 2002; Project Galileo, 2006; Thomas *et al.*, 1997, 1997a; Zuber *et al.*, 2000]. In this context, the computation of stable and unstable manifolds of periodic orbits, as done using continuation techniques in [Calleja, Doedel, Humphries *et al.*, 2012], could prove useful in the design of inexpensive orbit transfers. Results could be useful for asteroid mining missions, a far-reaching goal to mine large amounts of rare, precious elements that can be found on small asteroids close to the Earth, of which there are at least seven thousand [Blair, 2000; Gerlach, 2005].

Acknowledgments

The work of VAR and EJD was supported by NSERC Canada. VAR also received support from the Canadian Space Agency. VAR also thanks Dr. T. Jannson of the Physical Optics Corporation for their support.

6. REFERENCES

Arribas, M., Elipe, A. [2001] "Non-integrability of the motion of a particle around a massive straight segment," *Physics Letters A* **281**, pp. 142-148.

Bartczak, P., Breiter, S. [2003] "Double material segment as the model of irregular bodies," *Celestial Mechanics and Dynamical Astronomy* **86**, pp. 131-141.

Blair, B. R., [2000] "The Role of Near-Earth Asteroids in Long-Term Platinum Supply," *Space Resources Roundtable* **2**, pp. 5-19.

Britt, D. T., Yeomans, D., Housen, K., Consolmagno, G.J. [2002] "Asteroid density, porosity, and structure," in: *Asteroids III*, eds. Bottke Jr., W.F., Cellino, A., Paolicchi, P., and Binzel, R.P. (University of Arizona Press, Tucson), pp. 485-500.

Calleja, R., Doedel, E. J., Humphries A. R., Lemus-Rodríguez A., Oldeman E. B., [2012] "Boundary-Value Problem Formulations for Computing Invariant Manifolds and Connecting Orbits in the Circular Restricted Three Body Problem," *Celestial Mechanics and Dynamical Astronomy* **114** (1-2), pp. 77-106.

Celletti, A., [2010] "Stability and Chaos in Celestial Mechanics," (Praxis Publishing, Chichester, UK)

Cellino, A., Di Martino, M., Drummond, J., Farinella, P., Paolicci, P., Zappalà, V. [1989] "Vesta's shape, density and albedo features," *Astronomy and Astrophysics* **219**, pp. 320-321.

Davoust, E. [1986] "Periodic orbits in elliptical galaxies," *Astronomy and Astrophysics* **156**, pp. 152-156.

Davoust, E. [1983] "Periodic orbits in elliptical galaxies," *Astronomy and Astrophysics* **125**, pp. 101-108.

Dichmann, D. J., Doedel, E. J., Paffenroth, R. C. [2003] "The computation of periodic solutions of the 3-body problem using the numerical continuation software AUTO, " in *Libration Point Orbits and Applications*, eds. Gómez, G., Lo, M. W., & Masdemont, J. J. (World Scientific) pp. 429-488.

Doedel, E. J., Romanov, V. A. [2012] "Periodic orbits associated with the libration points of the homogeneous rotating gravitating triaxial ellipsoid," *Int. J. Bifurcation and Chaos* **22**(10), 20 pp.

Doedel, E. J., Oldeman, B. E. [2011] "AUTO-07P, Continuation and Bifurcation Software for Ordinary Differential Equations," (Concordia University, Canada)

Doedel, E. J., Romanov, V. A., Paffenroth, R. C., Keller, H. B., Dichmann, D. J., Galán, J., Vanderbauwhede, A. [2007] "Elemental periodic orbits associated with the libration points in the circular restricted 3-body problem," *Int. J. Bifurcation and Chaos* **17**(8), pp. 2625-2677.

Doedel, E. J., Paffenroth, R. C., Keller, H. B., Dichmann, D. J., Galán, J., & Vanderbauwhede, A. [2003] "Continuation of periodic solutions in conservative systems with application to the 3-body problem," *Int. J. Bifurcation and Chaos* **13**(6), pp. 1-29.

Duboshin, G. N. [1959] "On one particular case of the problem of the translation-rotation motion of two bodies," *Sov. Astronomical Journal* **3**, pp. 154-165.

Elipe, A., Lara, M. [2006] "A simple model for the chaotic motion around asteroids," *Revista Mexicana de Astronomía y Astrofísica* **25**, pp. 3-6.

Elipe, A., Lara, M. [2004] "A simple model for the chaotic motion around (433) Eros," *Prepublicaciones del Seminaro Matemático García de Galdeano, Univ. de Zaragoza* **6**, pp. 1-15.

Elipe, A., Lara, M. [2003] "A simple model for the chaotic motion around (433) Eros," *Journal of the Astronomical Sciences* **54**, pp. 391-404.

Gerlach, C. L., [2005] "Profitably Exploiting Near-Earth Object Resources," *2005 Int. Space Development Conf., Washington, DC, May 19-22, 2005*, 56 pp.

Guttiérrez-Romero, S., Palasián, J., F., Yanguas, P. [2004] "The invariant manifolds of a finite straight segment," *Monografías de la Real Academia de Ciencias de Zaragoza* **25**, pp. 137-148.

Hu, W., Scheeres, D. J. [2002] "Spacecraft motion about slowly rotating asteroids," *Journal of Guidance, Control, and Dynamics* **25**, pp. 765-775.

Lara, M. [2003] "Repeat ground track orbits of the Earth tesseral problem as bifurcations of the equatorial family of periodic orbits," *Celestial Mechanics and Dynamical Astronomy* **86**, pp. 143-162.

Lara, M., Scheeres, D. J. [2003] "Determining stability regions in highly perturbed, non-linear dynamical system using periodic orbits," *Monografías del Seminario Matemático García de Galdeano, Univ. de Zaragoza* **27**, pp. 385-392.

Markeyev, A. P. [1978] The Libration Points in Celestial Mechanics and Space Dynamics (Nauka, Moscow). (*in Russian*)

Mitchell, D. L., Scott Hudson, R., Ostro, S., J., Rosema, K. D. [1998] "Shape of asteroid 433 Eros from inversion of Goldstone radar Doppler spectra," *Icarus* **131**, pp. 4-14.

Miller, J. K., Konopliv, A. S., Antreasian, J. J., *et al.* [2002] "Determination of shape, gravity, and rotational state of asteroid 433 Eros," *Icarus* **155**, pp. 3 -17.

Najid, N.-E., El ourabi, E. *et al.* [2011] "Analytical expression of the potential generated by a massive inhomogeneous straight segment," *SF2A-2011: Proc. of the Annual Meeting of the French Society of Astronomy and Astrophysics, Eds.: Alecian, G. , et al*, pp. 643 -646.

Najid, N.-E., El ourabi, E. *et al.* [2012] "Equilibria and Stability Around a Straight Rotating Segment with a Parabolic Profile of Mass Density," *The Open Astronomy Journal* **5**, pp. 19 -25.

Project Galileo [2006] Asteroid Gaspra; Asteroid Ida and Dactil. Available via www2.jpl.nasa.gov/galileo/slides/slide10.html and www2.jpl.nasa.gov/galileo/slides/slide18.html

Riguas, A., Elipe, A., Lopez-Moratalla, T. [2001] "Non-linear stability of the equilibria in the gravity field of a finite straight segment, " *Celestial Mechanics and Dynamical Astronomy* **81**, pp. 235-248.

Riguas, A., Elipe, A., Lara, M. [1999] "Periodic orbits around a massive straight segment," *Celestial Mechanics and Dynamical Astronomy* **73**, pp. 169-178.

Scheeres, D. J., Williams, B. G., Miller, J. K. [2000] "Evaluation of the dynamic environ of an asteroid: application to 433 Eros," *Journal of Guidance, Control, and Dynamics* **23**, pp. 466-475.

Scheeres, D. J., Ostro, S. J., Hudson, R. S., Werner, R. A. [1996] "Orbits close to asteroid 4769 Castalia," *Icarus* **121**, pp. 67-87.

Scheeres, D. J., [1994] "Dynamics about uniformly rotating triaxial ellipsoid: application to asteroids," *Icarus* **110**, pp. 225-238.

Thomas, P. C., Binzel, R. P., Gaffey, M. J., Storrs, A. D., Wells, E., Zellner B. H. [1997] "Impact excavation on the asteroid 4 Vesta: Hubble space telescope results," *Science* **277**, pp. 1492-1495.

Thomas, P. C., Binzel, R. P., Zellner B. H., Storrs, A. D., Wells, E., [1997a] "Vesta: spin pole, size and shape from HST images," *Icarus* **128**, pp. 88-94.

Zuber, M. T., Smith, D. E., Cheng, A. F., Garvin, J. B., *et al.* [2000] "The shape of 433 Eros from the NEAR-Shoemaker laser rangefinder," *Science* **289**, pp. 1788-1793.